Atomic structure of GTP cyclohydrolase I

ARTICLE *in* STRUCTURE · JUNE 1995

Impact Factor: 5.62 · DOI: 10.1016/S0969-2126(01)00179-4 · Source: PubMed

Atomic structure of GTP cyclohydrolase I

Herbert Nar[1*†], Robert Huber[1], Winfried Meining[2], Cornelia Schmid[2], Sevil Weinkauf[2] and Adelbert Bacher[2]

[1]Max Planck Institut für Biochemie, Abteilung Strukturforschung, Am Klopferspitz, D-82152 Martinsried, Germany and [2]TU München, Department of Chemistry, Lichtenbergstr. 4, D-85747 Garching, Germany

Background: Tetrahydrobiopterin serves as the cofactor for enzymes involved in neurotransmitter biosynthesis and as a regulatory factor in immune cell proliferation and the biosynthesis of melanin. The biosynthetic pathway to tetrahydrobiopterin consists of three steps starting from GTP. The initial reaction is catalyzed by GTP cyclohydrolase I (GTP-CH-I) and involves the chemically complex transformation of the purine into the pterin ring system.

Results: The crystal structure of the *Escherichia coli* GTP-CH-I was solved by single isomorphous replacement and molecular averaging at 3.0 Å resolution. The functional enzyme is a homodecameric complex with D_5 symmetry, forming a torus with dimensions 65 Å × 100 Å. The pentameric subunits are constructed via an unprecedented cyclic arrangement of the four-stranded antiparallel β-sheets of the five monomers to form a 20-stranded antiparallel β-barrel of 35 Å diameter. Two pentamers are tightly associated by intercalation of two antiparallel helix pairs positioned close to the subunit N termini. The C-terminal domain of the GTP-CH-I monomer is topologically identical to a subunit of the homohexameric 6-pyruvoyl tetrahydropterin synthase, the enzyme catalyzing the second step in tetrahydrobiopterin biosynthesis.

Conclusions: The active site of GTP-CH-I is located at the interface of three subunits. It represents a novel GTP-binding site, distinct from the one found in G proteins, with a catalytic apparatus that suggests involvement of histidines and, possibly, a cystine in the unusual reaction mechanism. Despite the lack of significant sequence homology between GTP-CH-I and 6-pyruvoyl tetrahydropterin synthase, the two proteins, which catalyze consecutive steps in tetrahydrobiopterin biosynthesis, share a common subunit fold and oligomerization mode. In addition, the active centres have an identical acceptor site for the 2-amino-4-oxo pyrimidine moiety of their substrates which suggests an evolutionarily conserved protein fold designed for pterin biosynthesis.

Structure 15 May 1995, **3**:459–466

Key words: biosynthesis, crystal structure, cyclohydrolase, GTP, tetrahydrobiopterin

Introduction

GTP cyclohydrolase I (E.C. 3.5.4.16) (GTP-CH-I) catalyzes the initial step in the biosynthesis of various pteridines such as skin and eye pigments, methanopterin, folic acid and tetrahydrobiopterin (BH_4) in a wide variety of organisms [1]. As a cofactor for the aromatic amino acid hydroxylases and nitric oxide synthase, BH_4 is involved in neurotransmitter biosynthesis [2–4]. Its synthesis is correlated with cytokine-mediated T-lymphocyte proliferation [5] and it is an essential regulator in melanin biosynthesis in epidermal tissue [6].

A variety of neuronal disorders are associated with altered levels of BH_4, including depression [7], Alzheimer's [8] and Parkinson's [9] diseases as well as inflammatory diseases, vitiligo and several other clinical syndromes [10]. Defects in GTP-CH-I cause hyperphenylalaninemia [11] and, very recently, analyses on a genetic level have shown that dopa-responsive dystonia, a variant form of parkinsonism, arises from genetic defects in the human GTP-CH-I gene [12].

The *de novo* biosynthesis of BH_4 (Fig. 1) starts with GTP, which is converted to dihydroneopterin triphosphate by GTP-CH-I in a complex series of reaction steps. Dihydroneopterin triphosphate is then transformed to 6-pyruvoyl tetrahydropterin by 6-pyruvoyl tetrahydropterin synthase (E.C. 4.6.1.10) (PTPS). Finally, this intermediate is stereospecifically reduced to BH_4 by the NADPH-dependent sepiapterin reductase (E.C. 1.1.1.153) [1].

GTP-CH-I is subject to genetic and post-translational regulation mechanisms reflecting the important role of BH_4 biosynthesis. GTP-CH-I biosynthesis in lymphocytes is induced by cytokines [5]. In rat liver, it is controlled by feedback inhibition via a BH_4-mediated complex formation with another protein, p35 [13]. Multiple mRNA forms of the enzyme have been detected in human, rat and *Drosophila melanogaster* [14,15]. In *Drosophila*, it has been shown that differential expression of various forms of the enzyme occurs throughout development and that these variant proteins differ in their N-terminal domains.

GTP-CH-I has been characterized from a number of sources including *Escherichia coli* [16] and several other microorganisms [17], *Drosophila* [18], and rat [19] and human [20] liver. Sequence information from bacterial, insect and mammalian species [21–24] suggests that the C-terminal part of cyclohydrolases has evolved conservatively; for example, the C-terminal 120 residues of the *E. coli* and human enzymes show 66% sequence homology.

*Corresponding author. †Present address: Dr Karl Thomae GmbH, Abteilung Chemische Forschung, Birkendorferstr. 65, 88357 Biberach, Germany.

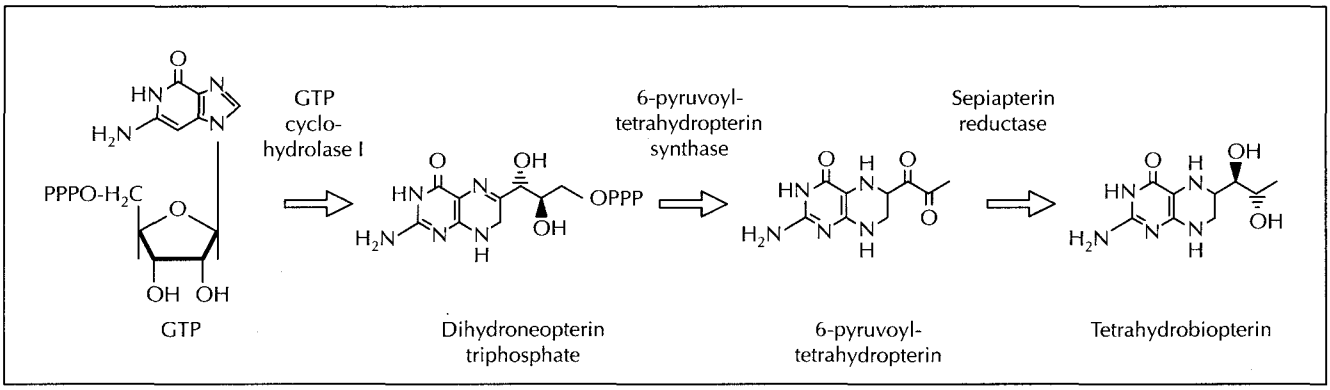

Fig. 1. Biosynthesis of tetrahydrobiopterin. The reaction catalyzed by GTP cyclohydrolase I involves release of the C8 atom of GTP as formate, an Amadori rearrangement of the sugar moiety, and ring closure via a Schiff base reaction.

Isolation, recombinant expression and crystallization of GTP-CH-I from *E. coli* has been reported [25]. Electron microscopy on freeze-etched crystal surfaces, in combination with X-ray crystallographic methods, has shown that the active enzyme is a homodecameric protein complex consisting of five-fold symmetric pentameric subunits. This combination of techniques has also revealed the approximate relative arrangement of the decamers in the crystal cell (W Meining *et al.*, unpublished data).

Recently, we determined the three-dimensional structure of recombinant rat liver PTPS, the enzyme catalyzing the second step in BH_4 biosynthesis [26]. We report here the X-ray crystal structure of GTP-CH-I, the enzyme catalyzing the first step, from *E. coli* at 3.0 Å resolution.

Results and discussion

Crystals of *E. coli* GTP-CH-I are obtained under various conditions [27]. The crystal species used for the present structure analysis is monoclinic with two decamers in the asymmetric unit. The structure was solved by single isomorphous replacement (SIR) and averaging techniques. Information about the packing arrangement obtained by electron microscopy (W Meining *et al.*, unpublished data) was helpful in the initial stages of crystallography. The refined model includes residues 3–24 and 29–217 of the 221-residue sequence of *E. coli* GTP-CH-I.

Monomer structure

The GTP-CH-I monomer folds into an α+β-structure [28] with a predominantly helical N-terminal part. An antiparallel helix pair, composed of helix h2 (residues 32–49) and helix h3 (residues 62–72), is remote from the main body of the molecule. The compact C-terminal domain (residues 95–217) comprises a sequential four-stranded antiparallel β-sheet including a 45-residue insertion between β-strands b2 and b3 which contains two antiparallel helices (h4 and h5) forming a layer on one side of the β-sheet. The C terminus is formed by a three-turn α-helix, positioned on the other side of the β-sheet. The N-terminal helix, h1 (residues 5–17), lies on top of helices h4 and h5 (Fig. 2).

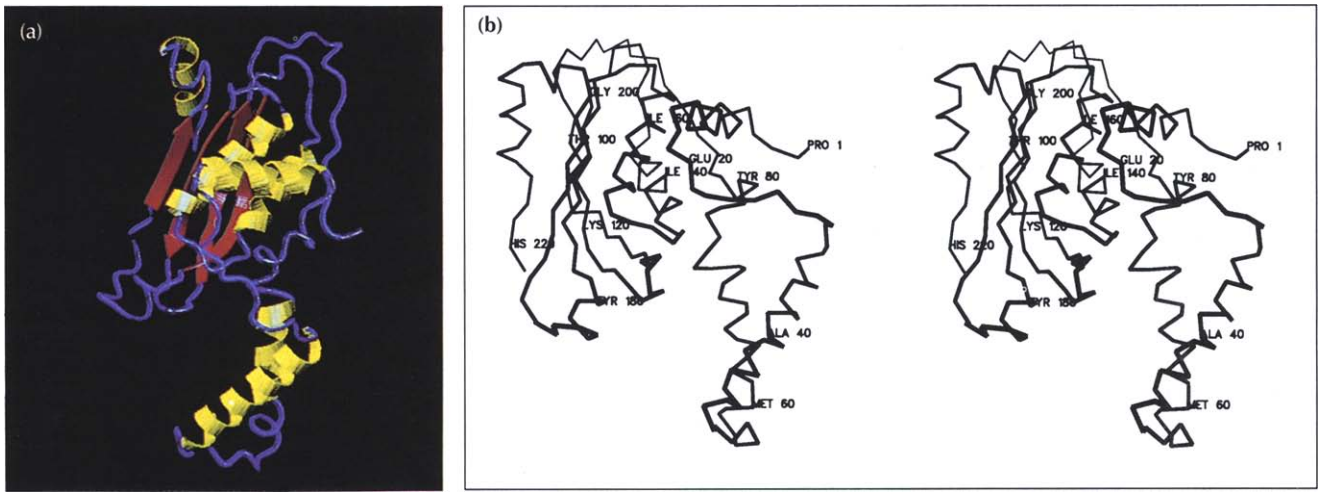

Fig. 2. The GTP-CH-I monomer. **(a)** Ribbon-type representation of the secondary-structure elements. The N terminus is to the right in this view of the molecule and the C terminus is hidden behind the β-sheet. Secondary-structure elements are colour coded (α-helices yellow, β-strands red and loop regions blue). **(b)** Stereo-plot with every 20th Cα atom labelled.

Pentamer structure

Five monomers associate in a highly symmetrical fashion along their β-sheets to form a 20-stranded antiparallel β-barrel with a diameter of 35 Å (Fig. 3). The N-terminal β-strand (b1) of one monomer thereby forms a hydrogen-bond ladder with the C-terminal β-strand (b4) of the neighbouring monomer. Within the pentamer, further interactions are mediated by two extended loop regions on the second monomer (residues 85–95 and 130–140) that interlock with a groove in the first monomer. The central cavity of the β-barrel is occupied by the C-terminal helices from each monomer, which form a parallel helix bundle with a diameter of ~15 Å between the helix centres. The pentamer has the overall shape of a crab with five 'legs' composed of the N-terminal helix pairs of the individual monomers (see Fig. 3b).

Decamer structure

The GTP-CH-I decamer is formed by face-to-face association of two pentamers. The 'legs' of one pentamer clasp the 'body' of the other, that is, the antiparallel helices h2 and h3 on one monomer are intertwined with those of another monomer, wedged into the cleft between the helix pair and the C-terminal domain. Because the arrangement of the two five-fold symmetric pentamers follows a two-fold symmetry, the decamer has perfect D_5 particle symmetry and is toroidal, with an approximate height of 65 Å and a diameter of 100 Å (Fig. 4). It encloses a cavity of dimensions 30 Å × 30 Å × 15 Å which is accessible through the pores formed by the five helix bundles in the centre of the pentamers, but has no openings at the decamer equator. This cavity is partially occupied by the four C-terminal residues Arg218, His219, His220 and Asn221, which are not defined in the electron density and are probably disordered.

Inspection of the buried surface area within a decamer shows that the most extensive interactions are made between two monomers on different pentamers across the dyad axis. Apart from a hydrophobic cluster enclosed by the helix pairs, there are numerous two-fold symmetric hydrogen bonds and salt bridges, which serve to stabilize the complex. It has been shown that the decamer can be dissociated into dimers under high salt conditions [16], in line with the observations made here. Reassociation occurs upon addition of GTP, suggesting that the active site is at the interface of two dimers in the active enzyme complex.

The sequence homology between bacterial and mammalian cyclohydrolases suggests that their tertiary and quaternary structures are very similar. The greater sequence variability of the N-terminal domain probably has no consequences for oligomerization as it is located at the decamer periphery.

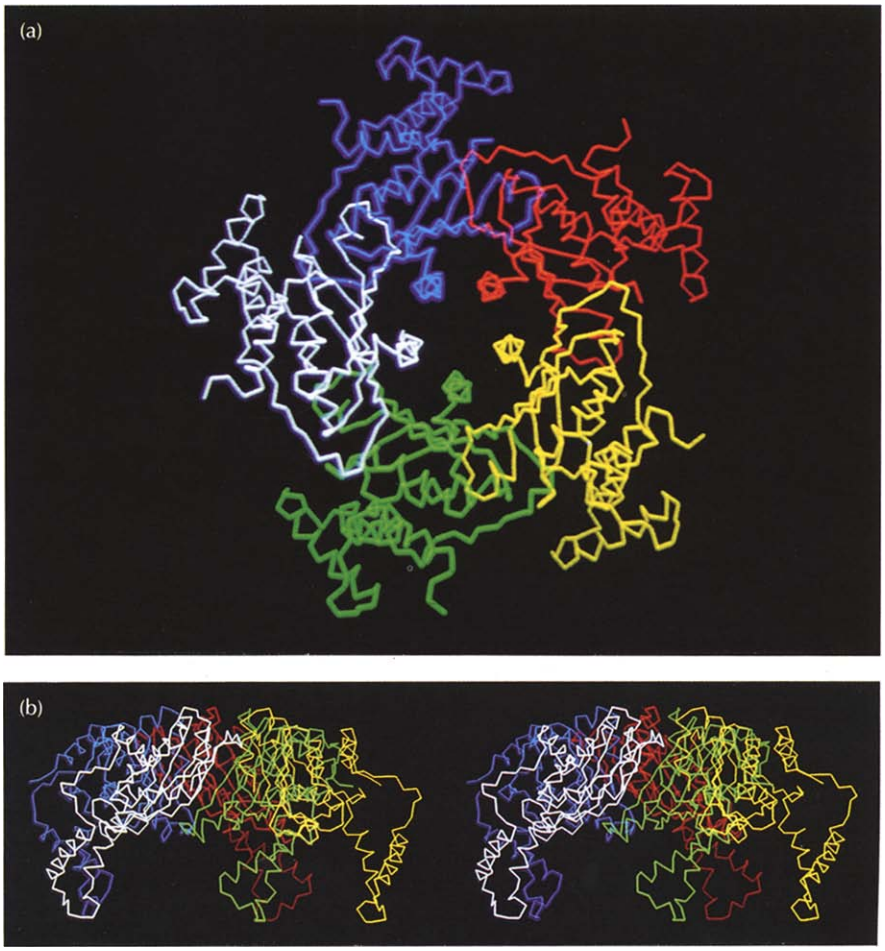

Fig. 3. The GTP–CH–I pentamer. **(a)** View of the pentamer along the five-fold symmetry axis. The individual monomers are shown in different colours. The centre of the structure consists of the C-terminal helices of the monomers which line a narrow pore of roughly 5–12 Å diameter. **(b)** Stereo-view of the pentamer in a Cα representation perpendicular to the five-fold symmetry axis. The antiparallel helix pairs of the individual subunits are remote from the compact C-terminal domain involved in pentamerization.

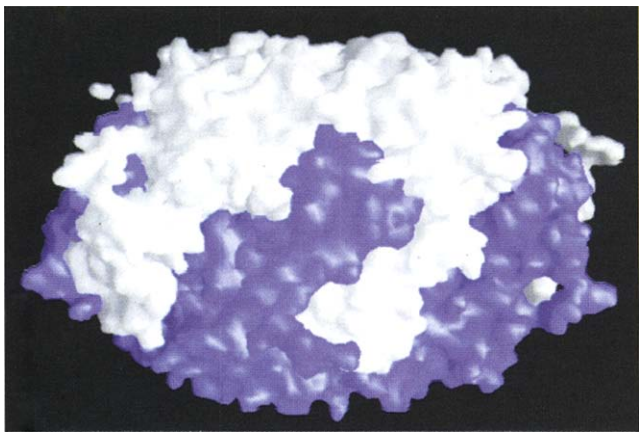

Fig. 4. Side view of the GTP-CH-I decamer showing the pentamer surfaces in different colours. Tight contacts are made by pairs of subunits between pentamers by intercalation of their helical domains.

Comparison with 6-pyruvoyl tetrahydropterin synthase

The structure of the C-terminal domain of GTP-CH-I (residues 95–200) is topologically identical to PTPS (Fig. 5). In the latter, this single domain comprises 140 residues. A structural alignment of identically positioned amino acids in the four β-strands and the two α-helices, h4 and h5, results in a root mean square (rms) fit between Cα-atom positions of 1.9 Å for 71 Cα atoms. Whereas the secondary-structure elements are strictly conserved between the two protein folds, three insertions and one deletion become apparent upon superposition of PTPS onto GTP-CH-I. Prolonged loop regions occur in PTPS between the first two β-strands, between b2 and h4, and between the two helices. In GTP-CH-I, b3 and b4 are connected by a 15-residue loop which is a tight turn in PTPS. Significant sequence homology between the two proteins cannot be recognized even after a topological alignment, with the exception of a few residues that are probably involved in purine and pterin binding (see below). The structural similarity of the two proteins extends beyond the level of tertiary structure. In PTPS, hydrogen bonding between three four-stranded β-sheets of neighbouring monomers leads to an assembly with a 12-stranded antiparallel β-barrel at its core. The same mode of association is used in GTP-CH-I for the formation of the 20-stranded β-barrel. To accomplish this barrel formation, the β-sheets in the respective monomers exhibit a distinctly different twist to fill a 120° (in PTPS) or a 72° (in GTP-CH-I) sector of the barrel.

Active-site structure

This topological similarity to PTPS also provides a clue to the location of the active site in GTP-CH-I. A rather narrow pocket is found at the interface of three monomers (two from within one pentamer, A and A′, one from the other pentamer, B) which is formed by residues 110–113, 150–153 and 179–185 (from A), 87–89 and 131–139 (from A′) and Arg65 and Lys68 (from B). In place of a metal-binding site in PTPS there is a disulphide bridge between Cys110 and Cys181 in GTP-CH-I. The inner wall of the pocket is composed of hydrophobic residues Val150 (from A) and Leu134 (from A′) and by His179 (from A). The structure is stabilized by a salt bridge between Arg153 and Glu111 — two residues that are in absolutely conserved sequence patches.

A cluster of basic residues at the entrance to the active site could serve to bind the triphosphate moiety of the substrate (GTP) and the product (dihydroneopterin triphosphate) (Fig. 6). Indeed, in an F_o–F_c difference electron-density map computed after the entire protein model was built and used for phasing, we found a strong positive peak close to Lys136, Arg139 and Arg185 which is probably an orthophosphate moiety bound to the protein.

Furthermore, we have obtained X-ray data for a complex of GTP-CH-I with dGTP (data not shown) which shows the putative GTP-binding mode. At the bottom of the active-site pocket, a strictly conserved glutamate residue is found (Glu152), positioned at the N-terminal end of an α-helix, which serves as a binding site for the pyrimidine moiety of GTP through formation of a salt bridge to its guanidino group. The C4 oxo-function is hydrogen bonded to the neighbouring main-chain amide NH. Glu107 in PTPS serves an analogous function as an acceptor site. The structural homology between the C-terminal domain of GTP-CH-I and PTPS therefore

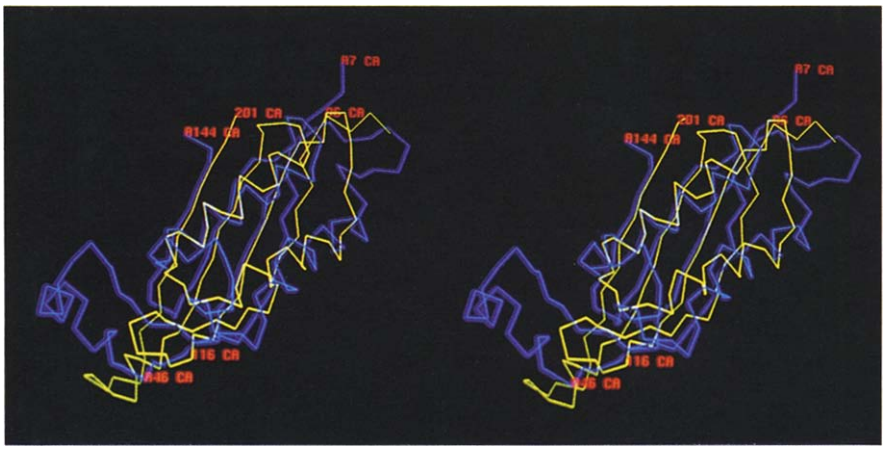

Fig. 5. Stereo superposition of the Cα traces of the C-terminal domain (residues 96–200) of GTP-CH-I (yellow) and 6-pyruvoyl tetrahydropterin synthase (PTPS) (blue). The fit between most atoms of both C-terminal β-strands and helix h5 (GTP-CH-I numbering) is perfect. Significant deviations occur in the N-terminal part of the domain (β-strands b1 and b2 and α-helix h4) where the distinct sheet twists become apparent.

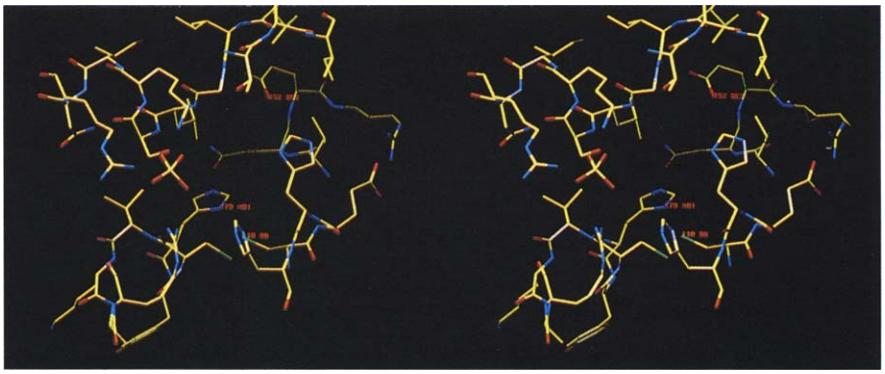

Fig. 6. Atomic structure of the putative active site of GTP-CH-I. A narrow pocket is enclosed by residues from three adjacent monomers. At the bottom of the pocket, Glu152 and the neighbouring main-chain amide NH serve as the acceptor site for the pyrimidine moiety of GTP. The disulphide bridge is flanked by three histidine residues (His112, His113 and His179) that may be involved in catalysis. Basic residues at the entrance to the cavity bind an orthophosphate group and may bind the γ-phosphate of the GTP triphosphate during catalysis.

suggests that this topology has been conserved to facilitate purine or pterin binding and modification.

The GTP-binding site found in GTP-CH-I is novel and differs from the generalized GTP-binding motif of G proteins. However, GTP-CH-I shares with G proteins a similar acceptor site for the pyrimidine functional group [29].

Because of the D_5 symmetry, there are 10 equivalent active sites per decamer. The minimum distance between these centres is 16 Å within a dimer. Kinetic studies on the enzyme from rat liver suggested that enzyme catalysis is subject to positive cooperativity. This was not observed for the *E. coli* enzyme [16]. The present structure of the 'resting' enzyme does not immediately suggest a mechanism for the phenomenon observed in the mammalian enzyme. The structural basis for the observed kinetic behaviour will have to await the structure analysis of one of the mammalian enzymes and of complexes of a GTP-CH-I with substrate and inhibitors.

The catalytic mechanism

The proposed catalytic mechanism of GTP-CH-I involves hydrolysis of the purine ring, requiring sequential cleavage of the N9–C8 bond and the N7–C8 bond in the N-formyl pyrimidine intermediate, with the release of C8 as formate [30,31]. An Amadori rearrangement of the ribose moiety could result in an intermediate with a C1′ methylene and a C2′ keto function which then would cyclize to the pterin ring system. The hydrolysis reactions, as well as the Amadori rearrangement, require acid–base chemistry only [32].

Residues which might be involved in catalysis are His112, His113 and His179 (Fig. 6). His112 is correctly placed for protonation of the ring oxygen of the ribose and might therefore initiate the rearrangement reaction. However, the presence of the cystine 110–181 in the active site of the cytosolic protein GTP-CH-I and, as inferred from the dGTP complex structure, its proximity to the imidazole portion of GTP are intriguing and could indicate an involvement of a cystine or a cysteine–thiol nucleophile in the ring hydrolysis step, for example, via a thiol/disulphide exchange prior to catalysis. *In vitro*, purine rings are very stable towards hydrolysis. Circumstantial evidence exists that chemical hydrolysis of GTP can be induced in the presence of mercaptoethanol, oxygen and Fe(II), which is consistent with the proposed involvement of the disulphide bond in catalysis [33].

Biological implications

Tetrahydrofolic acid and tetrahydrobiopterin are pteridines with important biological roles. The former serves as an enzyme cofactor in amino acid and purine biosynthesis, the latter is used as a cofactor in amino acid hydroxylation and in nitric oxide synthesis. Thus, both compounds are of clinical importance, for example, in cancer therapy and for treatment of neurological disorders. GTP cyclohydrolase I (GTP-CH-I) catalyzes the conversion of GTP into dihydroneopterin triphosphate. In bacteria, this intermediate enters the folic acid biosynthetic pathway. Vertebrates have lost the ability to synthesize folic acid and use this reaction as the initial step in tetrahydrobiopterin synthesis. Despite these distinct roles, bacterial and mammalian GTP cyclohydrolases I exhibit an extraordinarily high degree of sequence homology.

In order to gain insight into the molecular processes underlying pterin biosynthesis, we initiated a crystallographic program to study the three-dimensional structures of the participating enzymes. Recently, we showed that 6-pyruvoyl tetrahydropterin synthase (PTPS), the enzyme catalyzing the second step in tetrahydrobiopterin biosynthesis, is a homohexameric complex with unusual structural features. Oligomerization of subunits into trimers is facilitated by a three-fold symmetric arrangement resulting in the formation of a 12-stranded antiparallel β-barrel enclosing a highly positively charged pore.

Here, we describe the atomic structure of GTP-CH-I from *Escherichia coli*. The enzyme is a homodecameric complex of 250 kD, a dimer of pentamers, with overall dimensions of 65 Å × 100 Å. Despite the lack of sequence homology with PTPS, the C-terminal domain of a GTP-CH-I subunit is topologically identical to the PTPS subunit. In GTP-CH-I, pentamerization leads to the formation of a 20-stranded antiparallel β-barrel.

The active site is positioned at the interface of three subunits and consists of a novel GTP-binding site, which differs from the general binding motif of G proteins, and a catalytic apparatus that implicates three histidines and, possibly, a cystine in the reaction mechanism.

Because of the high degree of sequence homology between cyclohydrolases, the structures of the mammalian enzymes are probably very similar to the presented bacterial enzyme structure. Thus, it should be possible to gain a molecular understanding of the causes of genetic diseases associated with GTP-CH-I, such as Dystonia–Parkinson syndrome, by mapping the genetic lesions from patients to sites on the three-dimensional structure of the human enzyme obtained either experimentally or by homology modelling.

Furthermore, in combination with mutational analysis of the putative components of enzyme catalysis presented here, the three-dimensional structure of the *E. coli* GTP-CH-I provides a firm basis for gaining a detailed understanding of the enzymatic reaction mechanism. Finally, the information obtained in this study should aid in the interpretation of the complex biochemical regulation of tetrahydrobiopterin biosynthesis.

Materials and methods

Crystallization

GTP-CH-I was homologously overexpressed in *E. coli* and isolated and crystallized as previously described [25]. Briefly, the protein was purified by ion-exchange or affinity chromatography, dialyzed against 20 mM K,Na-phosphate, 5 mM EDTA, pH 7 and crystallized by vapour diffusion against 0.5 M Na-citrate, pH 7.4. The monoclinic crystals are of space group $P2_1$ with lattice constants a=204.2 Å, b=210.4 Å, c=71.8 Å, β=95.8°. The crystals diffract to better than 3.0 Å resolution. Assuming two decamers in the asymmetric unit, the packing coefficient is 3.1 $Å^3$ Da^{-1}.

Data collection and phasing

X-ray intensity data for GTP-CH-I crystals were measured on a FAST area detector system (Enraf-Nonius, Delft) and on an imaging plate system (MAR Research, Hamburg) both mounted on a Rigaku RU200 rotating anode. For the SIR analysis, a native data set and a Ta_6Br_{14} derivative data set were collected from one crystal specimen to a resolution of 6.0 Å on the FAST system. This strategy was employed because of a slight but significant non-isomorphism of the native protein crystals. A 3.0 Å resolution data set was obtained from a different crystal measured on the imaging plate. FAST data were scaled and reduced with MADNES and ABSCOR [34,35]. Imaging plate data were processed with MOSFLM [36] and programs from the CCP4 suite [37]. All further crystallographic computing was performed with PROTEIN [38]. Heavy-atom positions were determined from difference Patterson functions and refined. Data collection and SIR phasing statistics are summarized in Table 1.

Molecular averaging

The orientations of the particle five-fold axes of the two decamers per asymmetric unit were found using Patterson space self-rotation functions. They are oriented along (ψ=90°,ϕ=84°) and (ψ=90°,ϕ=96°), that is, both are parallel to the ac plane and inclined at either +6° or –6° to the normal onto the ab plane.

The heavy-atom model of the SIR analysis, in conjunction with results obtained by freeze-fracture electron microscopy on the ab crystal plane, suggested that one Ta_6Br_{14} cluster bound in the centre of each of the four GTP-CH-I pentamers in the asymmetric unit. The vectors between two cluster-binding sites thus gave a crude estimate of the orientation and position of the two particle five-fold symmetry axes.

The exact location and orientation of the local symmetry axes was computed using the SIR map by direct space rotation and translation searches. The position and orientation of the particle five-fold axes were alternately varied in steps of 0.1 Å and 0.1° and the correlation coefficient optimized using the solvent flattened SIR electron density computed on a 1 Å grid. The electron-density map was then five-fold cyclically averaged using MAIN [39]. At this stage, no use was made of the particle two-fold axes nor of the identity between the two decamers in the asymmetric unit. The correlation coefficient for the local two-fold axes was used as a control over the progress of the averaging procedure (correlation R-factor: R_{start}=29%, R_{end}=53%; averaging R-factor: R_{start}=43%, R_{end}=25%).

The averaged decamer electron density was used to refine the position and orientation of the two particles in the asymmetric unit against the second data set using AMoRe [40]. This procedure was followed because the local symmetry operators, obtained as above, did not lead to convergence in the averaging and phase-extension protocol using the higher-resolution data set collected from the second native crystal. A general

Table 1. Data collection statistics.

Derivative	No. of measurements	Unique reflections	Resolution (Å)	Completeness (%) overall/last shell	R_M†	R_F‡	No. of sites	Phasing power§ (20.0–6.0 Å)	Figure of merit (20.0–6.0 Å)
NATI (FAST)	23 487	10 022	6.0	60/30	10.3	4.0			
TABR*	21 933	9599	6.0	56/16	11.6	4.4	4	1.84	0.52
NATI (IP)	209 458	111 785	3.0	93/84	9.9	5.6			

*Derivative soaking conditions: 5 mM Ta_6Br_{15} for 30 min. †$R_M = \Sigma|I_h - \langle I_h \rangle| / \Sigma \langle I_h \rangle$. ‡$R_F$ is R_M after independent averaging of Friedel pairs. §Phasing power: $\langle F_H \rangle / E$, where $\langle F_H \rangle = \Sigma\sqrt{(f_h^2/n)}$ is the root mean square heavy-atom structure-factor amplitude, $E = \Sigma\sqrt{[(F_{PHC} - F_{PH})^2/n]}$ is the residual lack-of-closure error with F_{PH} being the structure-factor amplitude and $F_{PHC} = F_P + f_H$, the calculated structure factor of the derivative.

molecular replacement procedure then confirmed the previously obtained decamer arrangement. In addition, the least-squares fitting procedure in AMoRe yielded new and improved centres of gravity and orientations of the two decamers in the asymmetric unit.

Model building and refinement

With an improved envelope derived from a skeletonized model of the averaged map and the refined local symmetry operators, it was possible to extend phases from 6.0 Å to 3.3 Å by a cyclic averaging procedure, again using just the five-fold symmetry information. The atomic model of a GTP-CH-I monomer could be built unambiguously into the 3.3 Å electron density with O [41]. The two independent decamers were constructed using the local symmetry information. Conventional refinement using X-PLOR version 3.1 [42] resulted in a model with R=18.9% for 98% of the data between 6.0 Å and 3.0 Å. The current model consists of residues 3–24 and 29–217, 15 water molecules and one orthophosphate per monomer. The two N-terminal residues, the four C-terminal residues and a short loop comprising residues 25–28 are not defined in the electron density, probably due to dynamic disorder. All residues have main-chain dihedral angles in allowed regions of the Ramachandran plot. The B-factors were refined individually with restraints on bonded and angle-related atoms and additional restraints based on the non-crystallographic symmetry (B_{av}=27.2 Å^2, rms B_{bonded}=4.4 Å^2). The rms deviations from standard values of bond length and angles are 0.008 Å and 1.59°, respectively. The 20 monomers per asymmetric unit were kept nearly identical during refinement, allowing an rms deviation of atomic positions of only 0.07 Å. Likewise, the two decamers appear to be identical in terms of their particle symmetry elements.

We have deposited the coordinates of *E. coli* GTP-CH-I in the Brookhaven Protein Data Bank.

Acknowledgements: This work was supported by the EC grant ERBCHRXCT 930243 (Pteridines: Biosynthesis, regulation and pharmacology), the Deutsche Forschungsgemeinschaft and the Fonds der chemischen Industrie.

References

1. Nichol, C.A., Smith, G.K. & Duch, D.S. (1985). Biosynthesis and metabolism of tetrahydropterin and molybdopterin. *Annu. Rev. Biochem.* **54**, 729–764.
2. Kaufman, S. & Fisher, D.B. (1972). Pterin-requiring aromatic amino acid hydroxylases. In *Molecular Mechanisms of Oxygen Activation: Pteridine Requiring Aminoacid Hydroxylases.* (Hayashi, O., ed), pp. 285–369, Academic Press, New York.
3. Tayeh, M.A. & Marletta, M.A. (1989). Macrophage oxidation of L-arginine to nitric oxide, nitrite and nitrate. Tetrahydrobiopterin is required as a cofactor. *J. Biol. Chem.* **264**, 19654–19658.
4. Kwon, N.S., Nathan, C.F. & Stuehr, D.J. (1989). Reduced biopterin as a cofactor in the generation of nitrogen oxides by murine macrophages. *J. Biol. Chem.* **264**, 20496–20501.
5. Ziegler, I. (1990). Production of pteridines during hematopoiesis and T-lymphocyte proliferation: potential participation in the control of cytokine signal transmission. *Med. Res. Rev.* **10**, 95–114.
6. Schallreuter, K.U., *et al.*, & Ziegler, I. (1994). Regulation of melanin biosynthesis in the human epidermis by tetrahydrobiopterin. *Science* **263**, 1444–1446.
7. Curtius, H.C., Niederwieser, A., Levini, R.A. & Lovenberg, W. (1983). Successful treatment of depression with tetrahydrobiopterin. *Lancet* **1**, 657–658.
8. Sawada, M., Hirata, Y., Arai, H., Iizuka, R. & Nagatsu, T. (1987). Tyrosine hydroxylase, tryptophane hydroxylase, biopterin and neopterin in the brains of normal controls and patients with senile dementia of Alzheimer type. *J. Neurochem.* **48**, 760–764.
9. Fujishiro, K., Hagihara, M., Takahashi, A. & Nagatsu, T. (1990). Concentrations of neopterin and biopterin in the cerebrospinal fluid of patients with Parkinson's disease. *Biochem. Med. Metab. Biol.* **44**, 97–100.
10. Duch, D.S. & Smith, G.K. (1991). Biosynthesis and function of tetrahydrobiopterin. *J. Nutr. Biochem.* **2**, 411–423.
11. Blau, N., Thoeny, B., Heizmann, C.W. & Dhondt, J.L. (1993). Tetrahydrobiopterin deficiency: from phenotype to genotype. *Pteridines* **4**, 1–10.
12. Ichinose, H., *et al.*, & Nagatsu, T. (1994). Heredetary progressive dystonia with marked diurnal fluctuation caused by mutations in the GTP cyclohydrolase I gene. *Nature Genet.* **8**, 236–242.
13. Harada, T., Kagamiyama, H. & Hatakeyama, K. (1993). Feedback regulation mechanisms for the control of GTP cyclohydrolase I activity. *Science* **260**, 1507–1510.
14. Togari, A., Ichinose, H., Matsumoto, S., Fujita, K. & Nagatsu, T. (1992). Multiple messenger RNA forms of human GTP cyclohydrolase I. *Biochem. Biophys. Res. Commun.* **187**, 333–338.
15. McLean, J.R., Krishnakumar, S. & O'Donnell, J.M. (1993). Multiple messenger RNAs from the punch locus of *Drosophila melanogaster* encode isoforms of GTP cyclohydrolase I with distinct N-terminal domains. *J. Biol. Chem.* **268**, 27191–27197.
16. Yim, J. & Brown, G.M. (1975). Characteristics of guanosine triphosphate cyclohydrolase I purified from *Escherichia coli. J. Biol. Chem.* **251**, 5087–5094.
17. Blau, N. & Niederwieser, A. (1985). GTP cyclohydrolases: a review. *J. Clin. Chem. Clin. Biochem.* **23**, 169–176.
18. Weisberg, P.E. & O'Donnell, J.M. (1986). Purification and characterization of GTP cyclohydrolase I from *Drosophila melanogaster. J. Biol. Chem.* **261**, 1453–1458.
19. Hatakeyama, K., Harada, T., Suzuki, S., Watanabe, Y. & Kagamiyama, H. (1989). Purification and characterization of rat liver GTP cyclohydrolase I. Cooperative binding of GTP to the enzyme. *J. Biol. Chem.* **264**, 21660–21664.
20. Schoedon, G., Redweik, U. & Curtius, H.C. (1989). Purification of GTP cyclohydrolase I from human liver and production of specific monoclonal antibodies. *Eur. J. Biochem.* **178**, 627–634.
21. Katzenmeier, G., Schmid, C. & Bacher, A. (1990). Cloning and expression of the putative gene coding for GTP cyclohydrolase I from *Escherichia coli. FEMS Microbiol. Lett.* **54**, 231–234.
22. Katzenmeier, G., Schmid, C., Kellermann, J., Lottspeich, F. & Bacher, A. (1991). Biosynthesis of tetrahydrofolate. Sequence of GTP cyclohydrolase I from *Escherichia coli. Biol. Chem. Hoppe Seyler* **372**, 991–997.
23. Hatakeyama, K., Harada, T., Shuhei, S., Yasuyoshi, W. & Kagamiyama, H. (1991). Cloning and sequencing of cDNA encoding rat GTP cyclohydrolase I, the first enzyme of tetrahydrobiopterin biosynthetic pathway. *J. Biol. Chem.* **266**, 765–769.
24. Guetlich, M., Schott, K., Werner, T., Bacher, A. & Ziegler, I. (1992). Species and tissue specificity of mammalian GTP cyclohydrolase I messenger RNA. *Biochim. Biophys. Acta* **1171**, 133–140.
25. Schmid, C., Ladenstein, R., Luecke, H., Huber, R. & Bacher, A. (1992). Crystallization and preliminary crystallographic characterisation of GTP cyclohydrolase I from *Escherichia coli. J. Mol. Biol.* **226**, 1279–1281.
26. Nar, H., Huber, R., Heizmann, C.W., Thoeny, B. & Buergisser, D.B. (1994). Three-dimensional structure of 6-pyruvoyl tetrahydropterin synthase, an enzyme involved in tetrahydrobiopterin biosynthesis. *EMBO J.* **13**, 1255–1262.
27. Schmid, C., *et al.*, & Bacher, A. (1993). Studies on GTP cyclohydrolase I of *Escherichia coli.* In *Chemistry and Biology of Pteridines and Folates.* (Ayling, J.E., Nair, M.G. & Baugh, G.M., eds), pp. 157–162, Plenum Press, New York.
28. Orengo, C.A. & Thornton, J.M. (1993). Alpha plus beta folds revisited: some favoured motifs. *Structure* **1**, 105–121.
29. Bourne, H.R., Sanders, D.A. & McCormick, F. (1991). The GTPase superfamily: conserved structure and molecular mechanism. *Nature* **349**, 117–127.
30. Shiota, T., Baugh, C.W. & Myrick, J. (1969). The assignment of structure to the formamido pyrimidine nucleoside triphosphate precursor of pteridines. *Biochim. Biophys. Acta* **192**, 205–210.
31. Wolf, W.A. & Brown, G.M. (1969). The biosynthesis of folic acid. Evidence for an Amadori rearrangement in the enzymatic formation of dihydroneopterin triphosphate from GTP. *Biochim. Biophys. Acta* **192**, 468–478.
32. Paulsen H. & Pflughaupt, K.W. (1985). The Amadori rearrangement. In *The Carbohydrates: Chemistry and Biochemistry IB.* (Pigman, W. & Horton, D., eds), pp. 899–904, Academic Press, New York.
33. Shiota, T., Palumbo, M.P. & Tsai, L. (1967). A chemically prepared formamido pyrimidine derivative of guanosine triphosphate as a possible intermediate in pteridine biosynthesis. *J. Biol. Chem.* **242**, 1961–1967.

34. Messerschmidt, A. & Pflugrath, J.W. (1987). Crystal orientation and X-ray pattern prediction routines for area-detector diffractometer systems in macromolecular crystallography. *J. Appl. Crystallogr.* **20**, 306–315.
35. Messerschmidt, A., Schneider, M. & Huber, R. (1990). ABSCOR: a scaling and absorption correction program for the fast area detector. *J. Appl. Crystallogr.* **23**, 436–439.
36. Leslie, A.G.W. (1991). Macromolecular Data Processing. In *Crystallographic Computing V.* (Moras, D., Podjarny, A.D. & Thierry, J.C., eds), pp. 27–38, Oxford University Press, Oxford.
37. Collaborative Computational Project, Number 4 (1994). The CCP4 suite: programs for protein crystallography. *Acta Crystallogr. D* **50**, 760–763.
38. Steigemann, W. (1974). Die Entwicklung und Anwendung von Rechenverfahren und Rechenprogrammen zur Strukturanalyse von Proteinen [PhD Thesis]. TU München, Germany.
39. Turk, D. (1992). Weiterentwicklung eines Programms für Molekülgraphik und Elecktronendichte-Manipulationen [PhD Thesis]. TU München, Germany.
40. Navazza, J. (1994). AMoRe: an automated package for molecular replacement. *Acta Crystallogr. A* **50**, 157–163.
41. Jones, T.A., Bergdoll, M. & Kjeldgaard, M. (1990). O: a macromolecule modelling environment. In *Crystallography and Modelling Methods in Molecular Design.* (Bugg, C. & Ealick, S., eds), pp. 189–199, Springer-Verlag, New York.
42. Brünger, A.T. (1992). *X-PLOR Version 3.1. A System for X-ray Crystallography and NMR.* Yale University, New Haven, CT.

Received: **22 Feb 1995**; revisions requested: **10 Mar 1995**; revisions received: **24 Mar 1995**. Accepted: **28 Mar 1995.**